

# 450 mm dual frequency capacitively coupled plasma sources: Conventional, graded, and segmented electrodes

Yang Yang<sup>1,a)</sup> and Mark J. Kushner<sup>2,b)</sup>

<sup>1</sup>Department of Electrical and Computer Engineering, Iowa State University, Ames, Iowa 50011, USA

<sup>2</sup>Department of Electrical Engineering and Computer Science, University of Michigan, 1301 Beal Avenue, Ann Arbor, Michigan 48109-2122, USA

(Received 1 September 2010; accepted 15 October 2010; published online 10 December 2010)

Wafer diameters for microelectronics fabrication will soon transition from 300 to 450 mm at a time when excitation frequencies for capacitively coupled plasmas (CCPs) are increasing to 200 MHz or higher. Already for 300 mm tools, there is evidence that wave behavior (i.e., propagation, constructive, and destructive interference) affects the uniformity of processing. The increase in diameter to 450 mm is likely to exacerbate these effects, perhaps requiring nontraditional tool designs. This is particularly important in dual frequency (DF) CCP tools in which there are potential interactions between frequencies. In this paper, results from a two-dimensional computational investigation of Ar plasma properties in a 450 mm DF-CCP reactor, incorporating a full-wave solution of Maxwell's equations, are discussed. As in 300 mm DF-CCP reactors, the electron density collapses toward the center of the reactor with increasing high frequency (*HF*), however, with more pronounced finite wavelength effects. Graded conductivity electrodes with multilayer of dielectrics are computationally demonstrated as a possible means to suppress wave effects thereby increasing plasma uniformity. Segmentation of the *HF* electrode also improves the plasma uniformity by making the electrical distance between the feeds and the sheath edges as uniform as possible.

© 2010 American Institute of Physics. [doi:10.1063/1.3517104]

## I. INTRODUCTION

The next generation of wafer size for microelectronics fabrication will be 450 mm in diameter with the transition from 300 mm wafers beginning as early as 2012.<sup>1</sup> One of the foreseeable challenges for this transition is the control of the uniformity of reactant fluxes onto wafers with areas 2.25 times that of 300 mm wafers. For dual frequency capacitively coupled plasma (DF-CCP) etching tools, this challenge on maintaining uniformity increases as the frequency of excitation increases due to electromagnetic (EM) and finite wavelength effects that become more severe as the electrode size increases.<sup>2</sup>

The application of high frequency (*HF*) radiofrequency (rf) sources in DF-CCP tools originates from the desire to separately control the magnitude of ion and radical fluxes, and ion energy distributions to the substrate.<sup>2-4</sup> Typically in DF-CCP reactors, power is applied at a low frequency (*LF*) to the bottom electrode (a few megahertz to 10 MHz) holding the wafer; and the *HF* is applied to the top electrode (tens of MHz to hundreds of MHz), although in some designs both the *LF* and *HF* are applied to the bottom electrode.<sup>5</sup> Power at the *LF* is intended to control the shape of the ion energy and angular distributions (IEADs) to the wafer. Power at the *HF* is intended to control the production of ions and radicals. Decoupling the two sources often requires that the sources be significantly different in frequency (e.g., *LF* < 10 MHz, *HF* > 100 MHz).<sup>6</sup>

Increasing the *HF* introduces EM wave effects which challenge the control of the uniformity of the plasmas.<sup>7-10</sup> These effects include constructive and destructive interference and skin effects. For example, the applied voltage applied to the rear of the electrode must propagate around the edges of the electrode to enter the plasma. Once entering the plasma, the electric field does not significantly penetrate into the conductive bulk plasma and is wave-guided in the sheath at the surface of the electrode. At sufficiently low frequency (long wavelength,  $\lambda$ ), the electric field uniformly appears across the sheath for an electrode of diameter  $d$ . For sufficiently high frequencies (short  $\lambda$ ), constructive interference of counter-propagating waves from opposite sides of the electrode increases the amplitude of the electric field in the sheath at the center of the electrode. This results in a center-high plasma density. These frequency dependent, finite-wavelength produced nonuniformities are already problematic for 300 mm plasma sources, and so will become increasingly problematic for 450 mm plasma sources.

In this article, we discuss results from a computational investigation of 450 mm DF-CCP reactors with plasmas sustained in Ar. As commercial 450 mm DF-CCP reactors are still under development, the reactor investigated in this article is scaled from the 300 mm tool discussed in Ref. 11 which also provides a baseline for comparison. We found that as with 300 mm plasma tools, the electron density in the 450 mm plasma tool transitions from center-and-edge high to center high with increasing *HF* (from 10 to 150 MHz), however this transition occurs at lower frequencies in concession to the smaller value of  $\lambda/d$ . These transitions result from a

<sup>a)</sup>Present address: Applied Materials Inc., 974 E. Arques Ave., Sunnyvale, CA 94085. Electronic mail: yang\_yang@amat.com.

<sup>b)</sup>Author to whom correspondence should be addressed. Electronic mail: mjku@umich.edu.

radial variation in the amplitude of the electric field in the sheaths which in turn modulates the electron energy distributions (EEDs).

The first technique investigated to address finite-wavelength effects is grading the conductivity of the surface of the *HF* electrode in contact with the plasma.<sup>12</sup> By decreasing the conductivity of the plasma-contacting dielectric surface of the electrode from the edge to center of the electrode, the EM wave can progressively propagate into the dielectrics. This changes the pattern of interference of the counter-propagating *HF* electric fields. The uniformity of the *HF* electric field and consequently, the plasma uniformity can be improved. The second technique is segmenting the *HF* electrode in order to equilibrate the distance from the rf feeds to the plasma sheath.<sup>13</sup> In doing so, the uniformity of plasma excitation with finite wavelengths can be improved.

The model used in this study is discussed in Sec. II. Parametric results from our investigation of properties of Ar plasmas sustained in DF-CCP reactors are presented in Sec. III. Possible strategies for improving plasma uniformity using graded conductivity and segmented electrodes are in Secs. IV and V. Our concluding remarks are in Sec. VI.

## II. DESCRIPTION OF THE MODEL

The model used in this investigation is the two-dimensional (2D) Hybrid Plasma Equipment Model which incorporates a full-wave solution of Maxwell's equations. The model is the same as that described in Refs. 11 and 14.

Briefly, continuity, momentum, and energy equations for neutrals and ions; continuity equations for electrons, and Maxwell's equations are integrated in time over many hundreds of rf cycles using acceleration techniques to obtain a periodic steady state. The resulting electric fields and ion fluxes to surfaces are periodically transferred to the electron Monte Carlo simulation (EMCS) module where the energy transport of bulk electrons and secondary electrons emitted from surfaces are addressed by computing EEDs as a function of position. Electron transport coefficients, temperatures, impact source functions and sources of secondary electron current obtained from the EMCS are returned to the fluid model. The process is iterated to convergence. During the last iteration, the electric fields and source functions for ions and neutrals are recorded as a function of position and phase in the rf cycle. With these values, the energy and angular distributions of ions and neutrals incident on the substrate are obtained using a Monte Carlo simulation. Powers are separately specified for the *LF* and *HF* sources, and the applied voltages are adjusted to deliver those powers.

The full set of Maxwell's equations is solved in the time domain, which enables investigation of the coupling between frequencies as well as intra-rf period feedback between plasma transport and the EM wave. In our model, we separately solve for the EM field (from rf sources) and the electrostatic (ES) field (from charges), and sum the fields for plasma transport. The solution method is described in detail in Ref. 11. The reaction mechanism for Ar plasmas is discussed in Ref. 15.

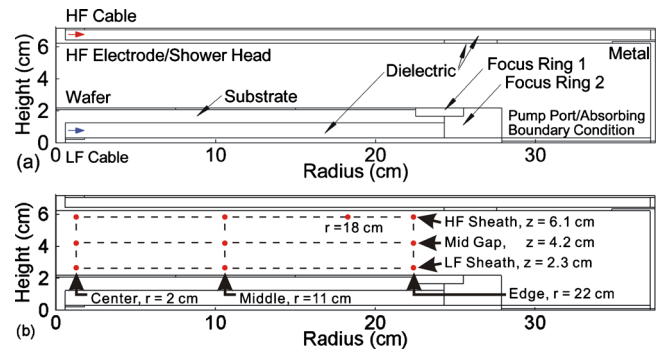


FIG. 1. (Color online) Properties of the 450 mm DF-CCP reactor. (a) Schematic showing the wafer on a substrate powered at low frequency surrounded by dielectric focus rings. The showerhead is powered at high frequency and is also surrounded by a dielectric. The *HF* and *LF* electric fields are launched into the reactor at the cable connections. (b) The radial and axial positions where EEDs will be plotted.

## III. PLASMA PROPERTIES OF 450 MM DF-CCP REACTORS

The model reactor used in this study is schematically shown in Fig. 1. A metal substrate powered at the *LF* (10 MHz) through a blocking capacitor is the bottom electrode. A conductive Si wafer ( $\sigma=0.01/\Omega$  cm), 45 cm in diameter, sits in electrical contact with the substrate which is surrounded by a Si ring (focus ring 1,  $\epsilon/\epsilon_0=12.5$ ,  $\sigma=10^{-6}/\Omega$  cm) and a dielectric focus ring (focus ring 2,  $\epsilon/\epsilon_0=8.5$ ,  $\sigma=10^{-8}/\Omega$  cm). Gas is injected through a shower head 48 cm in diameter that also serves as the *HF* electrode. The *HF* electrode is surrounded by a dielectric having  $\epsilon/\epsilon_0=1.0$  to simulate room air. All other surfaces in the reactor are grounded metal including the annular pump port.

The base case operating conditions are 50 mTorr of Ar with a flow rate of 600 sccm (sccm denotes cubic centimeter per minute at STP). The *LF* is held constant at 10 MHz, delivering a power of 450 W. The *HF* is varied from 10 to 150 MHz also with a constant power of 450 W. The *HF* and *LF* powers are fed into the reactor on the axis at the top and bottom of the reactor, respectively. So the EM waves are launched where the power cables are connected to the reactor, propagate through the surrounding dielectrics around the metal electrodes and into the plasma. Operating in this high frequency regime is particularly sensitive to the details of the design of the reactor, such as where the power is applied and the path the EM wave follows from the power cable to the plasma. As such, we are using this reactor for demonstration purposes, however we believe the trends will apply to this class of reactor.

### A. Electron density and EM fields

The electron density ( $[e]$ ) is shown in Fig. 2 for *LF* = 10 MHz (450 W) and *HF* = 10–150 MHz (450 W). The densities have been averaged over the *LF* cycle. The electron density transitions from being center-and-edge high for *HF* = 10–50 MHz (a dominant edge peak at 10 MHz), to center high at 100 and 150 MHz. The edge high plasma density,  $8 \times 10^{10}$  cm<sup>-3</sup>, at 10 MHz results from ES field enhancement at the periphery of the electrode. The center peaked electron density results from the constructive interference of counter-

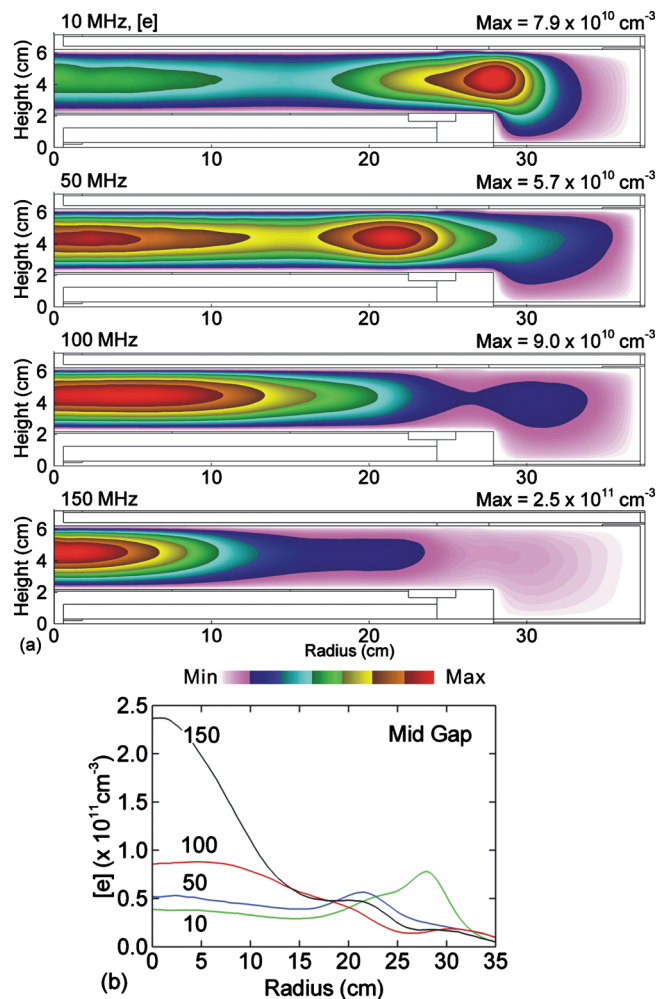


FIG. 2. (Color) Time averaged electron density ( $[e]$ ) for the base case conditions (Ar, 50 mTorr,  $P_{HF}=P_{LF}=450$  W,  $LF=10$  MHz). (a)  $HF=10, 50, 100, 150$  MHz and (b) radial  $[e]$  profile at the mid gap ( $z=4.2$  cm). The maximum value in each frame is noted. The electron density is plotted on a linear scale. The electron density transitions from being edge-and-center peaked at  $HF=10, 50$  MHz, to center peaked at 100 and 150 MHz.

propagating waves from the edges of the electrodes at the center of the reactor, a phenomenon we term the finite wavelength effect.<sup>11</sup> The transition from edge to center high plasma density with increasing  $HF$  is qualitatively similar to that in a 300 mm reactor but with a more prominent center peak due to the larger electrode size, and smaller value of  $\lambda/d$ . For example, at  $HF=50$  MHz, the electron density is center ( $5 \times 10^{10}$   $\text{cm}^{-3}$ ) and-edge-high ( $6 \times 10^{10}$   $\text{cm}^{-3}$ ) at 450 mm, while the center peak is usually absent or weaker in a 300 mm reactor due to a smaller finite wavelength effect. Exceeding 100 MHz, the collapse of the electron density toward the center of the reactor is more intense at 450 mm compared to a 300 mm reactor. For example, at  $HF=100$  MHz, the center plasma density is  $9 \times 10^{10}$   $\text{cm}^{-3}$  with center-to-edge ratio at the middle of the electrode gap of 3 at 450 mm and while being only about 2 in the 300 mm reactor.<sup>11</sup>

With increasing  $HF$ , the plasma effective wavelength decreases and the electric field launched by the  $HF$  source transitions from being largely ES to largely EM. (If not otherwise noted, references to the wave amplitude, phase, skin

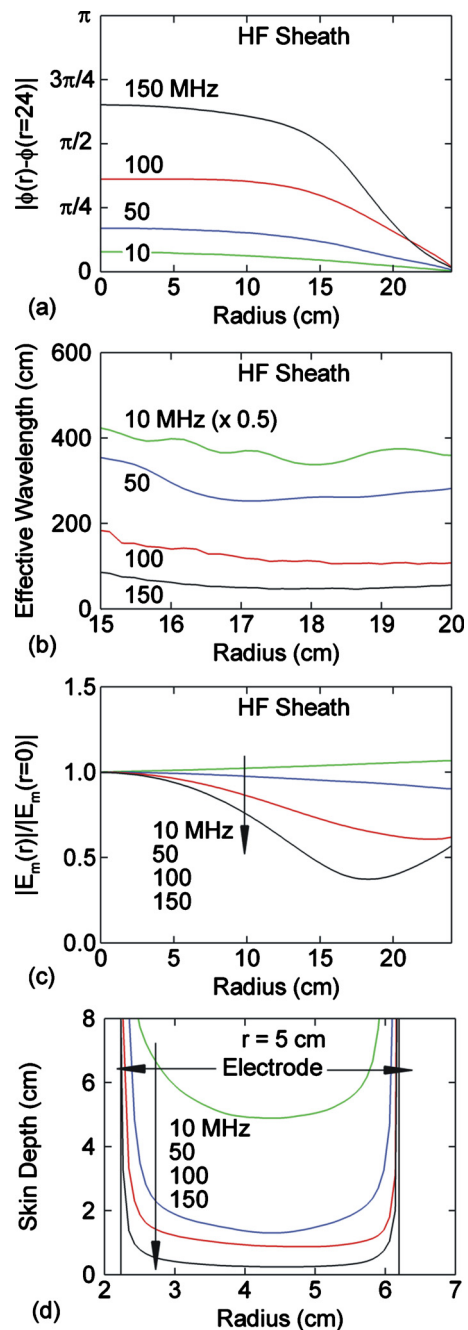


FIG. 3. (Color online) EM properties for the base case conditions (Ar, 50 mTorr,  $P_{HF}=P_{LF}=450$  W,  $LF=10$  MHz) and  $HF=10-150$  MHz. (a) Relative phase (with respect to the edge of the  $HF$  electrode) along the  $HF$  sheath, (b) plasma effective wavelength along the  $HF$  sheath, (c) magnitude of the  $HF$  field along the  $HF$  sheath (normalized by the magnitude at the center of the reactor) and (d) skin depth as a function of height at  $r=5$  cm. The  $HF$  field at 150 MHz has a minimum at about  $r=18$  cm.

depth and wavelength are for the  $HF$ .) This transition is partly indicated by the increasing phase change of the fundamental frequency of the axial EM field in the  $HF$  sheath with increasing  $HF$ , as shown in Fig. 3(a). At all  $HF$ , the phase change per cm diminishes toward the center of the reactor, which indicates a transition from a traveling wave to a standing wave due to constructive interference. (For standing waves, every point oscillates at the same phase).

The wave propagating inwards along the  $HF$  sheath is basically a surface wave whose wavelength was estimated by<sup>11</sup>

$$\lambda_{eff} = \frac{2\pi}{(\partial\phi/\partial r)}, \quad (1)$$

where  $\lambda_{eff}$  is the plasma effective wavelength and  $\partial\phi/\partial r$  is the derivative of the phase change in the radial direction. The estimated wavelengths in the *HF* sheath as a function of radius (from 15 to 20 cm) are shown in Fig. 3(b) for *HF* = 10–150 MHz. The wavelength decreases with increasing *HF* and the half-wavelength becomes commensurate to the electrode diameter for *HF* > 100 MHz.

As the wavelength decreases with increasing *HF*, the EM field in the *HF* sheath becomes increasingly center peaked due to constructive interference at the center of the reactor. This trend is shown in Fig. 3(c), where the magnitude of the *HF* electric field in the sheath is plotted as a function of radius for *HF* = 10–150 MHz. The fields are normalized by their values at  $r=0$ . At 10 MHz, the EM field is largely uniform with larger values near the periphery of the *HF* electrode resulting from ES edge enhancement. As the *HF* increases, the plasma effective wavelength decreases and the nonuniformity of the electric field therefore increases. At 150 MHz, the electrode radius is larger than the quarter-wavelength [the phase change from edge to center is also larger than  $\pi/4$ , as shown in Fig. 3(a)], so there is a minimum in the magnitude of the EM field at about  $r=18$  cm.

The skin depth also decreases with increasing *HF*, as expected. The skin depth as a function of height at  $r=5$  cm for *HF* = 10–150 MHz is shown in Fig. 3(d). The skin depth is given by<sup>16</sup>

$$\delta = \frac{1}{\omega\sqrt{\mu\varepsilon} \left\{ \frac{1}{2} \left[ \sqrt{1 + (\sigma/\omega\varepsilon)^2} - 1 \right] \right\}^{1/2}}, \quad (2)$$

where  $\omega=2\pi f$  is the angular frequency and  $\sigma$  the plasma conductivity. Note that this skin depth corresponds to the evanescent wave that propagates into the bulk plasma, not to the surface wave that propagates along the *HF* sheath. Exceeding 100 MHz, the skin depth in the bulk plasma is less than 1 cm, which is shorter than half the electrode separation. The local power deposition near the edges of electrodes as the EM wave propagates into the plasma tends to increase the local plasma density and is referred to as the skin effect. The skin effect usually dominates at lower frequencies (due to deeper penetration) or at higher pressures (stronger absorption). As the pressure is being held constant at 50 mTorr and the power deposition is moderate (450 W for each of *HF* and *LF* source), we did not observe a strong skin effect.

## B. EEDs and ionization sources

The EEDs near the center ( $r=2$  cm), middle ( $r=11$  cm for 50 MHz,  $r=11, 18$  cm for 150 MHz) and the edge of the electrodes ( $r=22$  cm) for *HF* = 50 MHz and 150 MHz are shown in Figs. 4 and 5. EEDs are shown at the edge of the *HF* sheath (height = 6.1 cm), mid gap (4.2 cm) and at the edge of the *LF* sheath (2.3 cm) (see Fig. 1 for these locations). At *HF* = 50 MHz, the EM field is relatively uniform along the *HF* sheath and consequently the EEDs are relatively uniform, as shown in Fig. 4(a). The tails of EEDs

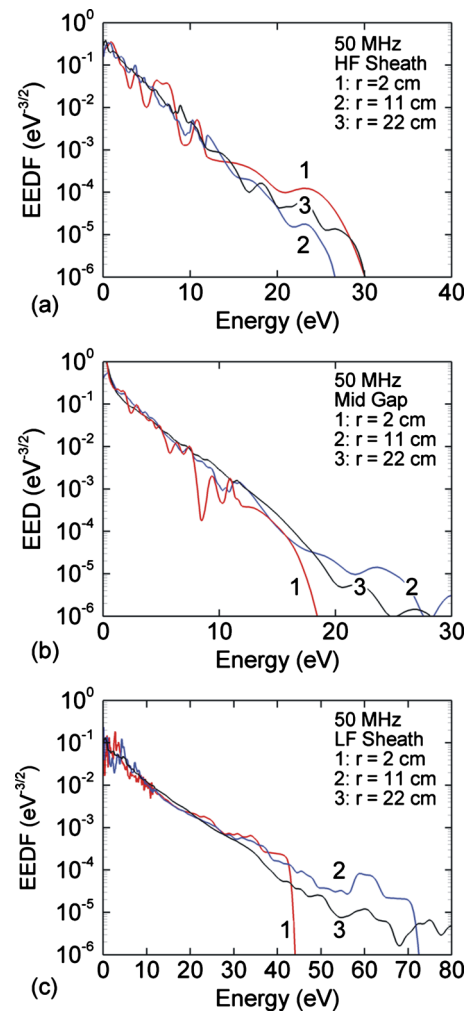


FIG. 4. (Color online) EEDs at different locations in the reactor for the base case conditions (Ar, 50 mTorr,  $P_{HF}=P_{LF}=450$  W,  $LF=10$  MHz) with *HF* = 50 MHz. (a) In the *HF* sheath, (b) at mid-gap, and (c) in the *LF* sheath. [These locations are shown in Fig. 1(b)].

at the center and near the edge of the *HF* electrode are slightly lifted, due to the finite wavelength effect and ES edge effect, respectively. In the bulk plasma and near the *LF* sheath, the ES edge effect at both the *LF* and *HF* are relatively important. As a result, the tails of EEDs in the bulk plasma and near the *LF* sheath are most prominent at large radii.

At 150 MHz, the plasma effective wavelength is shortened to such an extent that there is a minimum in the EM field at about  $r=18$  cm. This minimum in the sheath electric field is reflected in the EEDs along the *HF* sheath. The tails of the EEDs near  $r=18$  cm are most depressed, as shown in Fig. 5(a). The tails of EEDs in the *HF* sheath in the center of the reactor are lifted, resulting from the finite wavelength effect which produces a stronger electric field in the center of the reactor compared to the edge. With the skin depth being shorter than the electrode separation at 150 MHz, the penetration of *HF* wave into the bulk plasma is weak and the tails of EEDs at mid-gap in the center of the plasma are not enhanced. In fact, the EEDs in the bulk plasma near the edge of the *HF* electrode are lifted in the range of 0–20 eV, an effect most likely resulting from enhanced Ohmic heating in the low electron density region [Fig. 5(b)].

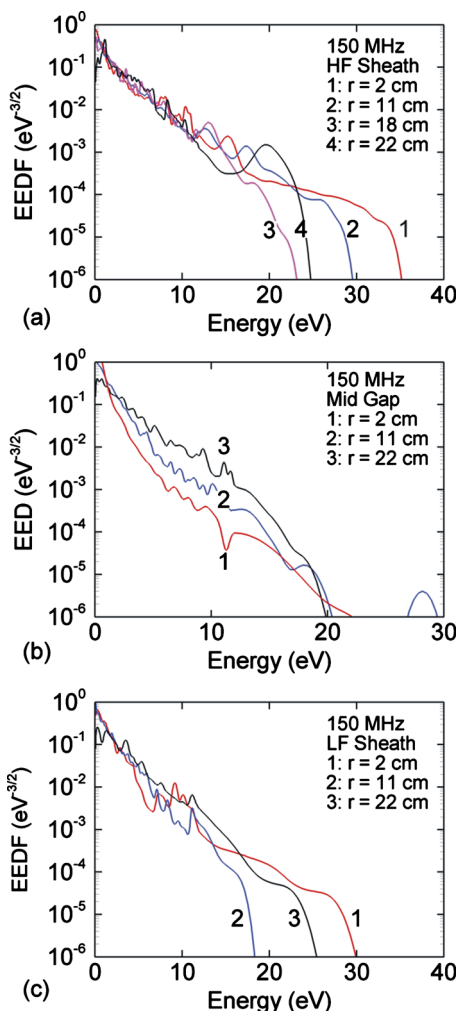


FIG. 5. (Color online) EEDs at different locations in the reactor for the base case conditions (Ar, 50 mTorr,  $P_{HF}=P_{LF}=450$  W,  $LF=10$  MHz) with  $HF=150$  MHz. (a) In the HF sheath, (b) at mid-gap, and (c) in the LF sheath. [These locations are shown in Fig. 1(b).] Near the center of the reactor, EEDs in the HF and LF sheath have more prominent tails due to the finite wavelength effect which increases the local sheath heating.

The HF wave can penetrate across the low electron density region near the edges of electrodes and then propagate along the LF sheath, as discussed in Ref. 11. So the electric field in the LF sheath is also modulated at the HF. The end result of this modulation by the HF electric fields, which are center peaked at 150 MHz, is that the tails of EEDs are lifted in the center of the reactor at the LF sheath, as shown in Fig. 5(c). Due to modulation of the LF fields, which are edge peaked, the tails of EEDs near the edge of the electrode are also lifted but to a lesser extent.

The electron impact ionization sources given by the sum of collisions by bulk and secondary, sheath accelerated electrons ( $S_i$ ) are shown in Fig. 6 for  $HF=50$  and 150 MHz. Maximum values are  $0.5\text{--}1.5 \times 10^{15} \text{ cm}^{-3} \text{ s}^{-1}$ . As the HF increases, there is a systematic shift in the maximum of  $S_i$  toward the HF electrode and toward the center of the reactor. We also observed a qualitatively similar shift in the 300 mm reactor discussed in Ref. 11. The shift toward the center of the reactor results from the constructive interference of the finite wavelength effect which increases the magnitude of the electric field in the HF sheath and so populates the tails of

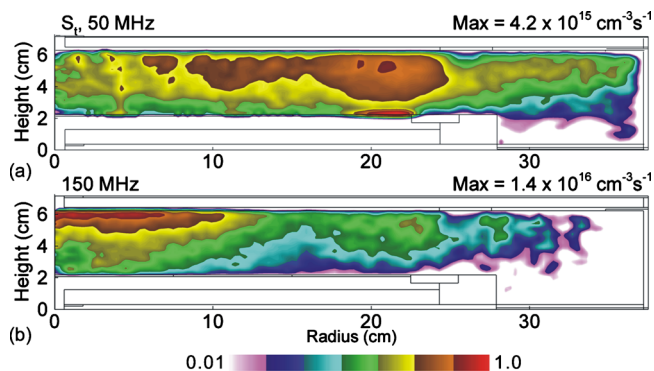


FIG. 6. (Color online) Time averaged electron impact ionization source ( $S_i$ ) by bulk and beam electrons for the base case conditions (Ar, 50 mTorr,  $P_{HF}=P_{LF}=450$  W,  $LF=10$  MHz) with (a)  $HF=50$  MHz and (b)  $HF=150$  MHz. The maximum value in each frame is noted.  $S_i$  is a log scale over two decades. With increasing HF, the maximum of  $S_i$  shifts toward the HF electrode due to enhanced sheath heating, and toward the center of the due to the finite wavelength effect. Note the minimum in  $S_i$  for 150 MHz near  $r=18$  cm due to the local minimum in electric field

the EEDs which are most responsible for ionization. The shift upwards toward the HF electrode can be attributed to at least two effects—the transition from bulk Ohmic heating to sheath heating as being the dominant source of power and a decrease in the skin depth. The local minimum in sheath electric field near  $r=18$  cm at 150 MHz [Fig. 3(c)] and decrease in tail of the EED [Fig. 5(a)] produce a local minimum in  $S_i$ .

### C. Ion flux and IEADs onto the wafer

The ultimate measure of uniformity, at least for materials processing, are the reactive fluxes and their energies incident onto the substrate. As the plasma transitions from center-and-edge high to center high with increasing HF, so does the  $\text{Ar}^+$  flux incident on the wafer, as shown in Fig. 7(a). The plasma density at the edge of the LF sheath, and the magnitudes of the LF and HF components in the lower sheath, ultimately determine the radial uniformity of IEADs onto the wafer. To show these dependencies, we separately collected IEADs over the center of the wafer (from  $r=0$  to 7.5 cm), over the middle of the wafer (from  $r=7.5$  to 15 cm) and over the edge of the wafer (from  $r=15$  to 22.5 cm). These IEADs for  $\text{Ar}^+$  are shown in Fig. 7(b) for  $HF=150$  MHz. As the plasma density and the HF field decrease from center to edge, the ES component of the LF sheath field decreases and the sheath thickness increases. The sheath transitions from a thick sheath at larger radius to a thin sheath at small radius. The IEADs of  $\text{Ar}^+$  are therefore systematically shifted down in energy with increasing radius.

### IV. GRADED CONDUCTIVITY ELECTRODE (GCE)

Methods to suppress EM wave effects and improve the plasma uniformity have been proposed. For example, in a system subject to the finite-wavelength effect, Sansonnens and Schmitt<sup>17</sup> fabricated a Gaussian-shaped surface profile on electrodes covered with a thin dielectric plate to confine the plasma in a constant interelectrode gap. A portion of the larger amplitude of the applied wave at the center of the

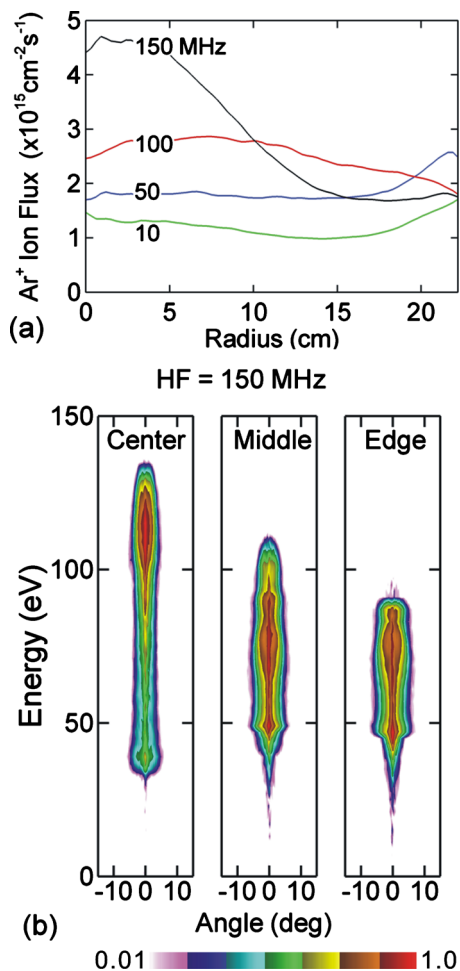


FIG. 7. (Color online) Ion flux and IEADs incident onto the wafer. (a) Ion flux for  $HF=10, 50, 100, 150$  MHz and (b) IEADs onto the wafer at  $HF=150$  MHz. The IEADs have units of per electron volt per steradian. The contours span two decades using a log scale. There is a large radial variation in ion flux and IEADs at 150 MHz due to the finite wavelength effect.

electrode was contained within the cavity, leaving a smaller amplitude of the electric field in the sheath. This reduced the center-high plasma density. This manipulation of EM fields to improve plasma uniformity has also recently been computationally demonstrated by Rauf *et al.*<sup>18</sup> In those investigations, a transmission line in contact with the bottom electrode in a  $HF$  CCP was used to vary the termination impedance for the EM field, and so channel return currents from the  $HF$  electrode to the side wall of the reactor. This enabled control of the location of the peak plasma density—from the center to the edge of the electrodes.

In this section, we apply a recently described method to suppress finite wavelength effects and so improve the plasma uniformity in 450 mm DF-CCP reactors by grading the conductivity of the surface of the electrode by contact with the plasma.<sup>13</sup> With this technique, the  $HF$  metal electrode is shielded from the plasma with a layer of lossy dielectric, the conductivity of which decreases from the edge to the center of the electrode. So as the  $HF$  EM wave propagates around the electrode and travels inwards along the surface of the dielectric toward the center of the electrode, the penetration of the  $HF$  electric field into the dielectric increases due to the decreasing conductivity. This leaves a smaller fraction of the

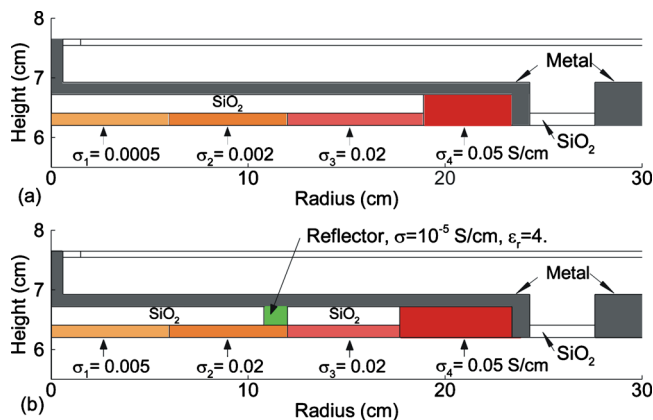


FIG. 8. (Color online) Geometry of GCE. (a) GCE1. The  $HF$  metal electrode is covered by a  $SiO_2$  plate (radius  $L=19$  cm), and Si segments with decreasing conductivity from edge to center. (b) GCE2. A dielectric ring (a radius of about 11 cm and a width of 1.2 cm) separates the  $SiO_2$  plate into two pieces. Wave reflection and refraction occur at the vertical surfaces of the dielectric ring.

potential to be dropped across the sheath and so counteracts the constructive interference of the  $HF$  electric field at the center of the reactor. The end result is a more uniform  $HF$  electric field in the sheath. We call this structure a graded conductivity electrode (GCE). Details of the design of GCEs are described in Ref. 13.

Application of the GCE to a DF-CCP, 450 mm reactor sustained in argon (GCE1) is shown in Fig. 8(a). As described in Ref. 13, a  $SiO_2$  plate ( $\epsilon/\epsilon_0=4.0$ ,  $\sigma=10^{-1} 1/\Omega$  cm, radius  $L=19$  cm) is sandwiched between the conductive dielectric surface and the metal electrode to provide an additional channel for wave propagation. The front surface of the electrode consists of an outer metal annulus ( $r=23.4$  cm to 24.3 cm), and four lossy dielectric annuli of decreasing conductivity. From edge to center, the conductivities are ( $1/\Omega$  cm), 0.05 ( $r=19$  to 23.4 cm), 0.02 ( $r=12$  to 19 cm), 0.002 ( $r=6$  to 12 cm), and 0.0005 ( $r=0$  to 6 cm). The operating conditions are 50 mTorr,  $HF$  of 150 MHz (450 W), and  $LF$  of 10 MHz (450 W).

With the conductivity of the surface layer lowest at the center of the reactor, the  $HF$  wave propagating along the  $HF$  sheath penetrates into the central segment into the  $SiO_2$  plate and then propagates outwards, being wave-guided by the  $SiO_2$  plate. The propagation of the wave in the  $SiO_2$  plate and penetration of the conductive segments are shown in Fig. 9, where the magnitude of the EM field ( $|E_{EM}|$ ) is plotted at 5 different phases of the  $HF$  wave as the wave propagates out of the rf cable into the reactor (during the second half of the  $LF$  cathodic cycle). There is a constant phase difference ( $1/26\pi$ ) between the frames.

Once the wave turns the corner of the metal electrode and enters the plasma, the wave propagates along the sheath at the top edge of the plasma. As the conductivity of the plasma facing materials decreases towards the center of the reactor, the wave penetrates deeper into those materials, and couples into the  $SiO_2$  layer. The wave is channeled by what appears to be a waveguide, and couples back into the sheath in the outermost, low conductivity segment.

As the outward traveling  $HF$  wave in the  $SiO_2$  cannot

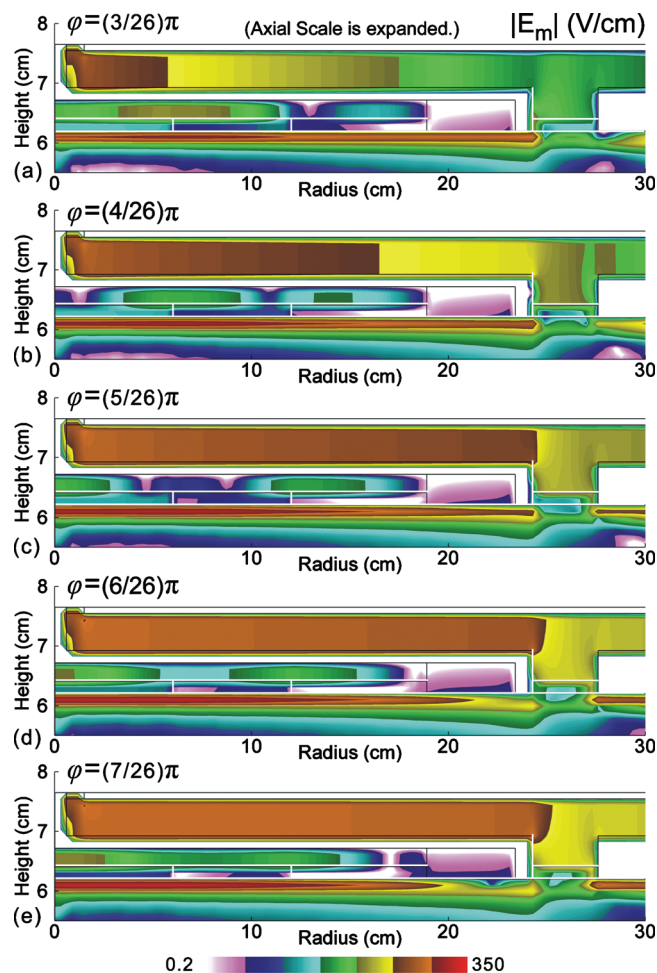


FIG. 9. (Color) The magnitude of the EM field ( $|E_{EM}|$ ) at five different phases (at the HF cable connection), during the second half of the LF cathodic cycle for GCE1 (Ar, 50 mTorr,  $P_{HF}=P_{LF}=450$  W,  $LF=10$  MHz,  $HF=150$  MHz). The phases are (a)  $(3/26)\pi$ , (b)  $(4/26)\pi$ , (c)  $(5/26)\pi$ , (d)  $(6/26)\pi$ , and (e)  $(7/26)\pi$ . The wave enters the SiO<sub>2</sub> plate through the central dielectric segment (the lowest conductivity).

penetrate through the outer segment (the most conductive or metal), it reflects and refracts at the periphery of the SiO<sub>2</sub> plate. Part of the wave propagates downwards and interferes with the local HF electric field. This interference is partly demonstrated in Fig. 10, where  $|E_{EM}|$  is plotted at four different HF phases during the second half of the LF cathodic cycle. The penetration of the wave through the conductive segment underneath the periphery of the SiO<sub>2</sub> plate perturbs the electric field in the local sheath, as shown in Fig. 10(a). The inward propagating surface wave then carries this perturbation toward the center of the reactor, as shown in Figs. 10(b)–10(d).

The interference shown in Fig. 10 was chosen to be destructive for the purpose of illustration. It turns out that on a time averaged basis, the interference increases the HF electric field near the periphery of the SiO<sub>2</sub> plate and so improves the uniformity of the HF electric field along the sheath. For example, the magnitude of the HF electric field in the sheath is shown in Fig. 11 as a function of radius for discharges with a conventional metal electrode (the case with HF=150 MHz in Sec. III) and with GCE1. With GCE1, a local maximum of the HF electric field is produced near the periphery of the SiO<sub>2</sub> plate.

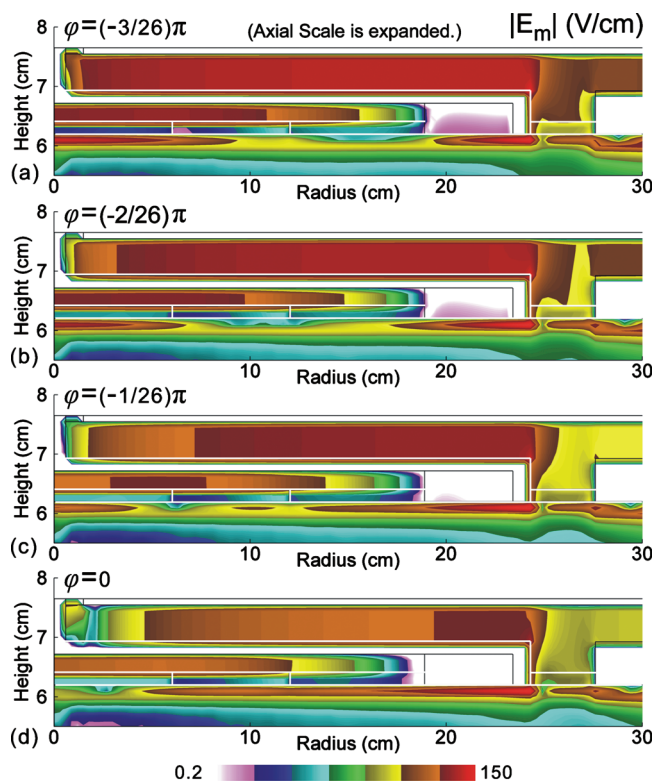


FIG. 10. (Color) Perturbation of the wave propagation in the SiO<sub>2</sub> plate to the HF electric field for different phases (at the HF cable connection) during the second half of the LF cathodic cycle for GCE1. (Ar, 50 mTorr,  $P_{HF}=P_{LF}=450$  W,  $LF=10$  MHz,  $HF=150$  MHz). (a)  $(-3/26)\pi$ , (b)  $(-2/26)\pi$ , (c)  $(-1/26)\pi$ , and (d) zero.

As the HF electric field is still center peaked with GCE1, one might expect that the electron density would also be center peaked. It turns out that as the wave propagates downwards near the periphery of the SiO<sub>2</sub> plate, the local bulk Ohmic heating is enhanced, which counteracts the center peaked sheath heating. As such, more ionization is produced around the periphery of the SiO<sub>2</sub> plate and the electron density becomes center-and-edge high, as shown in Fig. 12. Note that the discontinuities in conductivity between the inner three conductive segments cause refraction and reflection of the HF wave, which also induces downwards propagation and enhances bulk heating. As such, the total electron impact

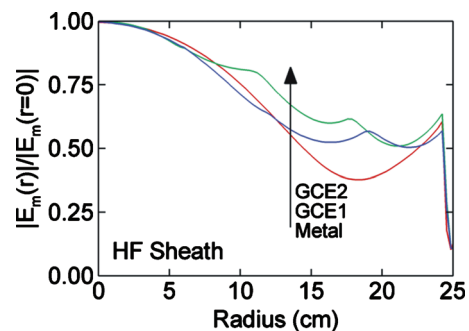


FIG. 11. (Color) Magnitude of the HF electric field in the HF sheath (normalized by the magnitude of the field at the center of the reactor) for discharges with different designs of electrode: the conventional metal electrode, GCE1 and GCE2. The operating conditions are Ar at 50 mTorr,  $P_{HF}=P_{LF}=450$  W,  $LF=10$  MHz, and  $HF=150$  MHz.

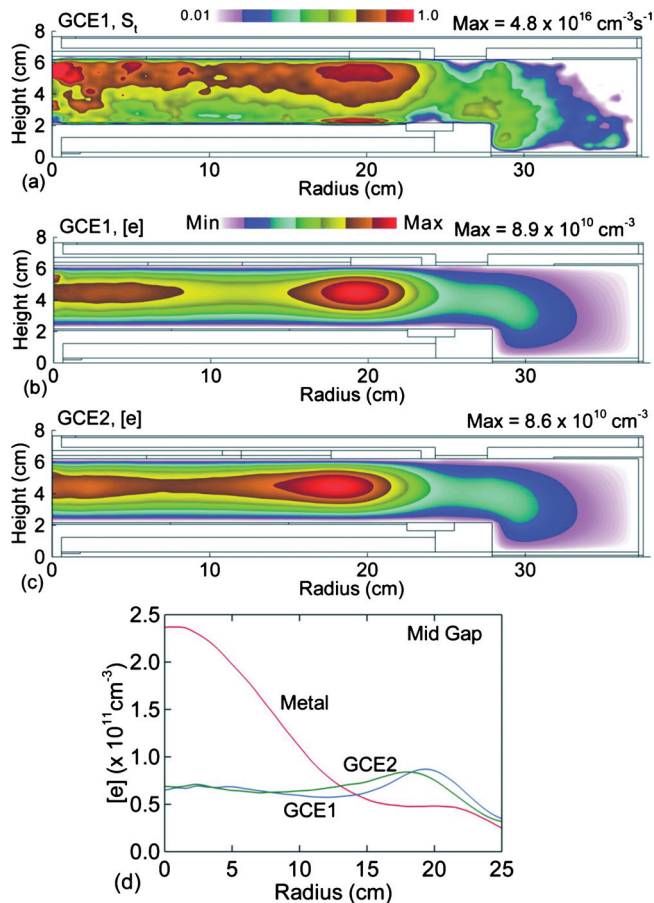


FIG. 12. (Color) Effects of GCE1 and GCE2 on plasma properties (Ar, 50 mTorr,  $P_{HF}=P_{LF}=450$  W,  $LF=10$  MHz,  $HF=150$  MHz). (a) Time averaged electron impact ionization source ( $S_i$ ) by bulk and beam electrons for GCE1, (b) time averaged electron density ( $[e]$ ) for GCE1, (c)  $[e]$  for GCE2, and (d) radial  $[e]$  profile at the mid gap ( $z=4.2$  cm). With GCE1, the heating of electron is both radially and axially more uniform compared to with the convention metal electrode [Fig. 6(b)]. For GCE2,  $[e]$  is increased at mid-radii compared to GCE1 and the plasma uniformity is further improved.

ionization source ( $S_i$ ) shown in Fig. 12(a) is more axially and radially uniform compared to the case with a metal electrode [Fig. 6(b)].

Designs such as GCE1 have some downsides, one being heating of the dielectrics. For our operating conditions, the central segment of GCE1 dissipates about 80 W, so additional cooling of the electrode may be necessary. Another downside is that a center-and-edge-high profile of  $[e]$  results and so we need to enhance the power deposition at mid-radii.

Here we take a lesson from the concept of a slot antenna in microwave engineering and place an annular dielectric ring at mid-radii between the metal electrode and the conductive surface, as shown in Fig. 8(b) (GCE2). The dielectric ring (at radius of about 11 cm with a width of 1.2 cm) cuts the  $\text{SiO}_2$  plate into two pieces and has a dielectric constant of 4.0 and conductivity of  $10^{-5}$   $1/\Omega$  cm. As the dielectric ring has a higher conductivity compared to  $\text{SiO}_2$ , wave reflection and refraction occurs at its vertical surfaces, which guides the wave to propagate downward. Behaving like a radiator, this dielectric ring enhances the  $HF$  electric field at mid-radii, as shown Fig. 11. As a result, with GCE2 the electron density is increased at mid-radii thereby being somewhat

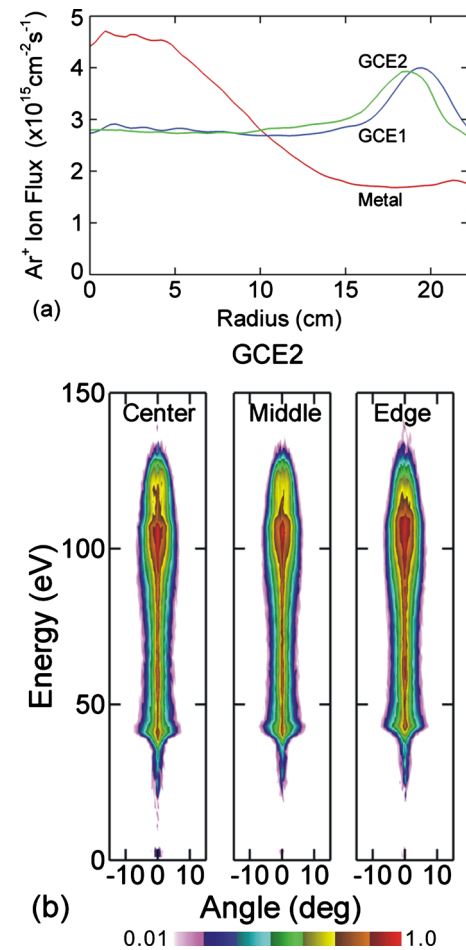


FIG. 13. (Color online) Ion flux and IEADs incident onto the wafer (Ar, 50 mTorr,  $P_{HF}=P_{LF}=450$  W,  $LF=10$  MHz,  $HF=150$  MHz). (a) Ion flux to the wafer for metal, GCE1 and GCE2 electrodes. and (b) IEADs to the center, middle and edge of the wafer with the GCE2 electrode. The IEADs have units of per electron volt per steradian. The contours span two decades using a log scale.

more uniform compared to GCE1, as shown in Figs. 12(c) and 12(d). The design of GCE2 also allows for less lossy dielectrics, which reduces electrode heating. With GCE2, the central segment dissipates about 15 W.

The improved plasma uniformity from GCEs translates into improved uniformity of the ion fluxes incident on the wafer. With GCE2, the maximum radial variation in  $\text{Ar}^+$  flux onto the wafer is within a factor of 1.3, as shown in Fig. 13(a) (compared to a factor of 3.2 with the metal electrode). As the uniformity of the thickness and the magnitude of the electric field in the  $LF$  sheath track that of the plasma, the uniformity of the IEADs incident on the wafer is also improved with GCE2, as shown in Fig. 13(b) (compare to Fig. 7 for IEADs with the metal electrode).

## V. SEGMENTED ELECTRODES

Another method that might be used to suppress EM wave effects in 450 mm reactors is to employ separately powered, segmented electrodes. Segmented electrodes have been proposed to achieve uniform excitation and are used in larger area plasma processing for liquid crystal digital panels, solar cells and microelectronics.<sup>12,19–21</sup> Uniform excita-

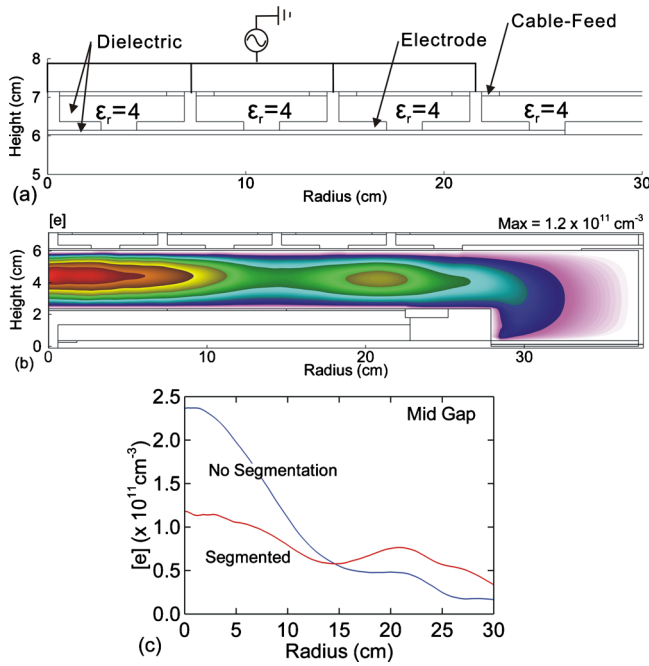


FIG. 14. (Color online) Geometry and electron density with a segmented electrode (Ar, 50 mTorr,  $P_{HF}=P_{LF}=450$  W,  $LF=10$  MHz). (a) Geometry, (b) 2D plot of time averaged electron density, and (c) radial  $[e]$  profile at the mid gap ( $z=4.2$  cm). The maximum electron density is  $1.2 \times 10^{11}$   $\text{cm}^{-3}$ , plotted on a linear scale.

tion with finite wavelengths can in principle be achieved if the distances from the rf feeds to the plasma sheath across the reactor are nearly equal. This may be achieved with segmented electrodes.

In this section, we discuss modeling results for separately powered, annular segmented electrodes in a 450 mm DF-CCP reactor sustained in Ar at 50 mTorr. In the first example, there are four annular segmented electrodes powered at 150 MHz with the same phase, each with a width of about 6 cm, as shown in Fig. 14. The segments are encased in a dielectric having  $\epsilon/\epsilon_0=4.0$ . A plate made from the same dielectric serves as the shower head and covers the surfaces of the four segments. The total power deposition of the four segments is held constant at 450 W. The substrate is powered at 10 MHz with a constant power of 450 W. Note that the designs presented here are conceptual and they would likely need further tuning for specific industrial applications.

As the four segments are separately powered, one might expect that there is no global surface wave propagating from the edge of the outmost segment toward the center of the reactor. It turns out that this is still the major mode of wave propagation. As such, the surface wave still constructively interferes at the center of the reactor, thereby increasing the magnitude of the local EM field, as shown in Fig. 15. Having said that, with segmentation (with in phase power) the HF field at large radii ( $r > 12$  cm) is increased relative to the on-axis value, which improves the uniformity across the HF sheath. The ratio of the unpowered area due to the spacing between segments to the powered area is largest at small radii. So the equal spacing between segments preferentially decreases the fraction of the total power dissipated near the center of the reactor.

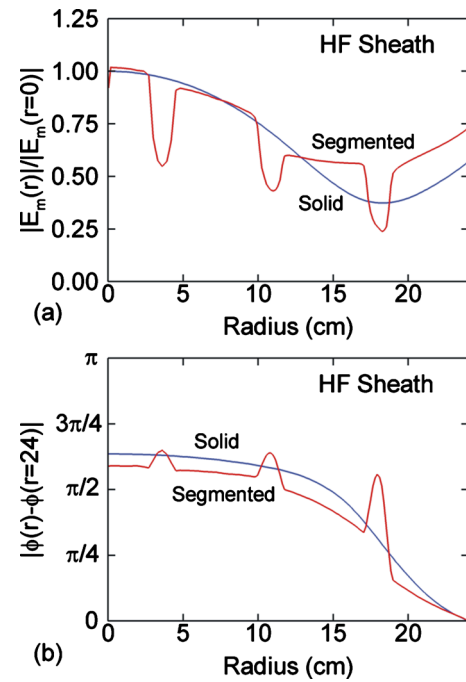


FIG. 15. (Color online) EM properties for discharges with a conventional metal electrode and the segmented electrode. (Ar, 50 mTorr,  $P_{HF}=P_{LF}=450$  W,  $LF=10$  MHz,  $HF=150$  MHz). (a) Magnitude of the HF field along the HF sheath (normalized by the magnitude at the center of the reactor) and (b) relative phase (with respect to the edge of the HF electrode) along the HF sheath. The electrical symmetry improves the radial uniformity of the HF electric field.

The end result of the improved uniformity of the HF field and reduced power deposition at the center of the reactor, is improved plasma uniformity, as shown in Figs. 14(b) and 14(c). Compared to the case with a solid electrode, the electron density at larger radii is increased and the profile is less center peaked. The uniformity of the ion flux incident onto the wafer and the uniformity of the IEADs are also improved as shown in Fig. 16.

To reduce the traveling wave and the constructive interference, the segments may have to be powered at different phases.<sup>19,20</sup> An example of the tuning of uniformity of the plasma by varying the phase of the segmented electrodes is shown by the electron densities in Fig. 17. Here we keep the voltages constant ( $LF=300$  V,  $HF=50$  V). The results in Fig. 17(a) were obtained with the phases of the four electrode segments being the same. The results in Fig. 17(b) were obtained with the phases of the segments alternating by  $180^\circ$ . The in-phase excitation retains the character of a surface wave propagating along the sheath and so has a center high plasma density. The out-of-phase excitation shifts the maximum plasma density to mid-radius. This middle-peaked plasma density could be a result of a higher order of waveguide mode being excited in the chamber. It is likely that real-time-control (strategies such as swapping the phases of the segments) will be required to tune or oscillate the phases of the segments to achieve maximum uniformity for a given set of process conditions.

## VI. CONCLUDING REMARKS

The properties of DF-CCP sources sustained in Ar for processing of 450 mm wafers have been computationally

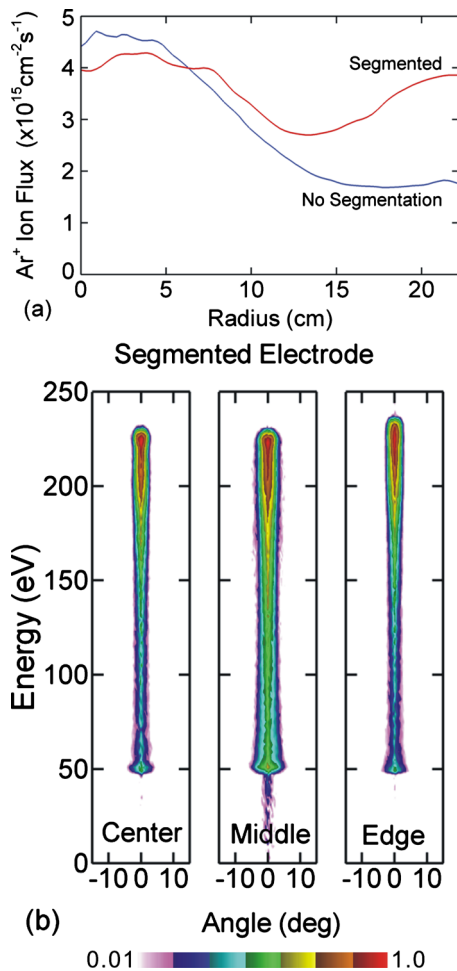


FIG. 16. (Color online) Ion flux and IEADs incident onto the wafer (Ar, 50 mTorr,  $P_{HF}=P_{LF}=450$  W,  $LF=10$  MHz,  $HF=150$  MHz). (a) Ion flux with a conventional electrode and with the segmented electrode. (b) IEADs for the discharge with the segmented electrode. The IEADs have units of per electron volt per steradian. The contours span two decades using a log scale. The segmented electrode produces more uniform IEADs.

investigated using results from a 2D plasma transport model. The model contains a time-domain solution of the full-wave, Maxwell equations to resolve EM and ES effects. The finite wavelength effect is more pronounced in the 450 mm reactor compared to 300 mm DF-CCP reactors, as indicated by the collapse of the plasma density toward the center of the reactor for  $HF$  exceeding 100 MHz. There is a minimum of the  $HF$  electric field in the sheath at mid radii at 150 MHz, likely due to that the radius of the electrode being larger than the plasma shortened quarter-wavelength. As the plasma density and the  $HF$  field decrease from center to edge at 150 MHz, the IEADs of  $Ar^+$  are systematically shifted down in energy with increasing radius.

An alternate design having GCEs was discussed. By covering the  $HF$  metal electrode with a layer of dielectric whose conductivity decreases from edge to center, with an additional layer of  $SiO_2$  between the metal electrode and the conductive surface, the radial uniformity of the  $HF$  electric field in the sheath is improved. The improvement is due, in part, to the capture of some of the electric potential of the wave in the dielectric, thereby leaving a smaller potential and electric field in the sheath. The wave enters the  $SiO_2$

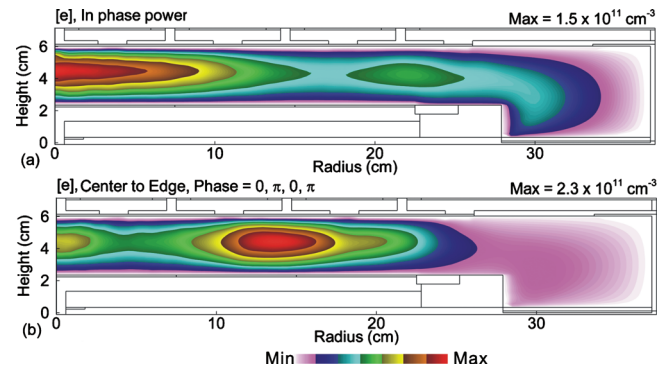


FIG. 17. (Color) Time averaged electron densities with segmented electrodes while holding voltages constant (Ar, 50 mTorr,  $V_{HF}=50$  V,  $V_{LF}=300$  V,  $LF=10$  MHz,  $HF=150$  MHz). (a) Segments are powered in phase. (b) Segments are powered with phases alternating by  $180^\circ$ . The plasma properties can be tuned by adjusting the phases of the segments.

plate through the central dielectric segment (the lowest conductivity) and propagates outwards, then reflects and refracts at the periphery of the  $SiO_2$  plate, which increases the local  $HF$  field on a time average basis. The downward propagation at the periphery of the  $SiO_2$  plate due to the local reflection and refraction also enhances the bulk electron heating, thereby increasing the local electron density. Adding a dielectric ring (with a higher conductivity than  $SiO_2$ ) introduces more vertical dielectric interfaces, which reflect and refract waves thereby enhancing the  $HF$  field at mid-radii. The uniformity of the plasma, ion fluxes and IEADs incident on the wafer is further improved.

Segmentation of the  $HF$  electrode provides the opportunity for increasing the plasma uniformity by reducing the distance from the cable feed to any location in the sheath. By separately powering the segments in the same phase, the  $HF$  wave still propagates from the outermost edge of the electrode segment toward the center of the reactor. But the uniformity of the  $HF$  field is improved as the distance from rf feeds to the plasma sheath are nearly equal. The ratio of the unpowered area due to the spacing between segments, to the powered area is largest at small radii, which decreases the fraction of the total power dissipated near the center of the reactor. The end result is that uniformity of the plasma, ion fluxes and IEADs incident on the wafer is improved. Tuning the phase of the segments will likely be required to optimize uniformity.

## ACKNOWLEDGMENTS

This work was supported by Applied Materials Inc., Tokyo Electron, Ltd., the Semiconductor Research Corp. and U.S. Department of Energy, Office of Fusion Energy Sciences (grants DE-SC0001939, DE-SC0002588).

<sup>1</sup>International Technology Roadmap for Semiconductor, 2009 edition. Retrieved from <http://www.itrs.net/>.

<sup>2</sup>S. Rauf, K. Bera, and K. Collins, *Plasma Sources Sci. Technol.* **17**, 035003 (2008).

<sup>3</sup>W. Tsai, G. Mueller, R. Lindquist, B. Frazier, and V. Vahedi, *J. Vac. Sci. Technol. B* **14**, 3276 (1996).

<sup>4</sup>K. Bera, S. Rauf, K. Ramaswamy, and K. Collins, *J. Appl. Phys.* **106**, 033301 (2009).

<sup>5</sup>T. Gans, J. Schulze, D. O'connell, U. Czarnetzki, R. Faulkner, A. R.

- Ellingboe and M. M. Turner, *Appl. Phys. Lett.* **89**, 261502 (2006).
- <sup>6</sup>T. Kitajima, Y. Takeo, Z. Ljpetrovic, and T. Makabe, *Appl. Phys. Lett.* **77**, 489 (2000).
- <sup>7</sup>M. A. Lieberman, J. P. Booth, P. Chabert, J. M. Rax, and M. M. Turner, *Plasma Sources Sci. Technol.* **11**, 283 (2002).
- <sup>8</sup>G. A. Hebner, E. V. Barnat, P. A. Miller, A. M. Paterson, and J. P. Holland, *Plasma Sources Sci. Technol.* **15**, 879 (2006).
- <sup>9</sup>P. Chabert, *J. Phys. D: Appl. Phys.* **40**, R63 (2007).
- <sup>10</sup>I. Lee, D. B. Graves, and M. A. Lieberman, *Plasma Sources Sci. Technol.* **17**, 015018 (2008).
- <sup>11</sup>Y. Yang and M. J. Kushner, *Plasma Sources Sci. Technol.* **19**, 055011 (2010).
- <sup>12</sup>Y. Yang and M. J. Kushner, *J. Phys. D* **43**, 152001 (2010).
- <sup>13</sup>A. R. Ellingboe, U.S. Patent No. 7,342,361 (11 March 2008).
- <sup>14</sup>M. J. Kushner, *J. Phys. D* **42**, 194013 (2009).
- <sup>15</sup>S. Rauf and M. J. Kushner, *J. Appl. Phys.* **82**, 2805 (1997).
- <sup>16</sup>C. A. Balannis, *Advanced Engineering Electromagnetics* (Wiley, New York, 1989), p. 149.
- <sup>17</sup>L. Sansonnens and J. Schmitt, *Appl. Phys. Lett.* **82**, 182 (2003).
- <sup>18</sup>S. Rauf, Z. Chen, and K. Collins, *J. Appl. Phys.* **107**, 093302 (2010).
- <sup>19</sup>B. Ellingboe, D. O'Farrel, C. Gaman, F. Green, N. O'Hara, and T. Michna, 62nd Gaseous Electronics Conference, Saratoga Springs, NY, October, 2009 [Bull. Am. Phys. Soc. **54**, BAPS.2009.GEC.KTP.3 (2009)].
- <sup>20</sup>K. Ryan and A. R. Ellingboe, 37th European Physics Society Conference on Plasma Physics, Dublin, Ireland, June 2010, p. 21.
- <sup>21</sup>M. Long, U.S. Patent No. 6,916,401 (12 July 2005).